Journal of Engineering Sciences, Assiut University, Vol. 38, No. 2, pp. 509-532, March 2010

CHARACTERIZATION OF A LOW-SPEED WIND TUNNEL SIMULATING URBAN ATMOSPHERES

Hamoud A. Al-Nehari*, Ali K. Abdel-Rahman**, Hamdy M. Shafey, and Abd El-Moneim Nassib****

Department of Mechanical Engineering, Faculty of Engineering, Assiut University, Assiut 71516, EGYPT

** Graduate Student, ** Associate Professor, *** Professor*

E-mail: h_nahary@hotmail.com

(Received January 19, 2010 Accepted February 15, 2010)

A new low-speed boundary-layer wind tunnel has been designed and constructed at the University of Assiut. A series of flow-characteristic evaluations were performed in this wind tunnel to determine the uniformity of flow and to verify its adequacy to simulate the atmospheric boundary layer (ABL) for environmental flow studies and pollutants dispersion in urban atmospheres. This paper presents the measurements of mean velocity and turbulence intensity distributions in the wind tunnel. The measurements showed uniform velocity distributions and low turbulence intensities at the entrance of boundary development section in the empty wind tunnel. The simulated ABL at the entrance of the test section using the Irwin's method that consists of a combination of spires and roughness elements has a thickness up to 500 m corresponding to urban area. The results show that the present wind tunnel is capable to maintain long run steady flow characteristics and reproducible flow patterns. In addition, the capability of the wind tunnel to simulate the flow in the urban area atmospheres is verified by comparing the measured mean velocity and turbulence intensity distributions against its counterparts obtained from Computational Fluid Dynamics (CFD) which employ two-equation k-ε turbulence model around and above buildings model. The numerical results agree well with the experimental data.

KEYWORDS: *Atmospheric boundary layer, Low speed-open loop wind tunnel, Wind tunnel characterization, Environmental flow.*

1. INTRODUCTION

Atmospheric boundary layer wind tunnels play an important role in many meteorological and engineering applications. Simulation of the atmospheric boundary layer in a wind tunnel is useful for environmental flow studies. There are two main reasons for simulating the atmospheric boundary layer in a wind tunnel. The first reason is to study the basic phenomena of micro-meteorological processes in the atmosphere. The second is to solve engineering problems of practical interest such as the dispersion of pollutants in complex terrain or in urban areas where buildings produce complex flow patterns. Wind tunnels are equipment designed to obtain airflow conditions, so that similarity studies can be performed, with the confidence that actual operational conditions will be reproduced. Once a wind

tunnel is built, the first step is to evaluate the flow characteristics and to examine the possibility of reproducing or achieving the flow characteristics for which the tunnel was designed.

NOMENCLATURE

Alphabetic Symbols

c_μ Constant
D Diameter of the turntable, m
H_C, H_M, H_T Heights of the computational domain, model, and wind tunnel respectively, m
I Turbulence intensity
k Turbulent kinetic energy, m^2/s^2
K_S Roughness height of the walls boundaries, m
L_C, L_M, L_T Lengths of the computational domain, model, and wind tunnel respectively, m
L_b Characteristic dimension of the building, m
p Mean static pressure, Pa
p_o Atmospheric pressure, Pa
Re Reynolds number, ($Re = u_\delta.x/\nu$)
s Model scale factor of a boundary layer simulation
u Mean axial velocity in x direction, m/s
u_e Mean velocity at the entrance of the boundary layer development section, m/s
u'_i ith fluctuating components of velocity, m/s
u_i ith mean velocity component, m/s
u_δ Mean axial velocity at height δ, m/s
V Magnitude of mean velocity, m/s
v Mean velocity in y direction, m/s
w Mean velocity in z direction, m/s
W_C, W_M, W_T Widths of the computational domain, model, and wind tunnel respectively, m
x Along-wind coordinate distance, m
x_i Cartesian coordinates, m
y Cross-wind (lateral) coordinate distance, m
z Vertical coordinate distance, m
z_o Aerodynamic roughness length, m

Greek Symbols

α The power law exponent
δ The boundary layer thickness, m
δ_{ij} Kronecker delta
ε Dissipation rate of the kinetic energy, m^2/s^3
ν Kinematic viscosity of fluid, m^2/s
ν_t Turbulent kinematic viscosity of flow, m^2/s
ρ Density of the air, kg/m^3
σ_k, σ_ε Turbulent Prandtl number for k and ε ($\sigma_k = 1.0$, $\sigma_\varepsilon = 1.3$)
σ_V Standard deviation of the turbulent velocity fluctuations, m/s

Many evaluation studies of wind tunnels are presented in the literature. Cook [1] described a wind tunnel of open-circuit configuration designed specifically for building aerodynamics. He examined and discussed the tunnel performance and indicated that it has some special features that assist the simulation of the atmospheric boundary layer. Sykes [2] designed and described a new wind tunnel of closed return configuration for industrial aerodynamic testing, and its performance is discussed. Counihan [3] developed a method for boundary layer simulation. The characteristics of this simulated boundary layer have been measured. A wind tunnel of closed-return configuration has been built at the University of Federal do Rio Gramde do Sul, Brazil, designed specifically to provide a testing facility for architectural and industrial aerodynamics [4]. A boundary layer wind tunnel at the Danish Maritime Institute in Lyngby is designed and described [5]. This wind tunnel is of the open-circuit type and

is integrated into a building raised for this purpose. Garg *et al*. [6] study the spectral description of the atmospheric boundary layers for appropriate modeling to investigate the wind effects on structures. It is concluded that proper estimation of the spectral parameters of the simulated Atmospheric Boundary Layers (ABLs) and their variation along the height of wind tunnel help in comparing the results obtained from different sources (wind tunnel tests) for identifying the influences of various flow/body parameters on the wind-induced effects and for formulating improved modeling of wind-structure interactions. Farell and Iyengar [7] discussed the simulation of atmospheric boundary layers using spires, a barrier wall, and a fetch of roughness elements in light of experiments carried out to reproduce the characteristics of a boundary layer for urban terrain conditions.

Comparisons of wind tunnel and atmospheric data are presented in many studies. Recent studies presented evaluation of flow characteristics in wind tunnel located at Northeast National University at Resiste Hncia (Chaco), Argentina [8, 9], and National University of Singapore [10]. Boundary-layer simulations are performed with help of grids, vortex generators and roughness elements, to facilitate the growth of the boundary layer. These are used in the most applied simulation methods, namely the full-depth simulation [3, 11, 12] and part-depth simulation [13, 14]. The use of jets and grids is also applied [11].

The purpose of this paper is to present results of measurements performed to evaluate the flow characteristics of the wind tunnel located at Laboratory of Environmental Studies and Research at the Mechanical Engineering Department of Assiut University, Assiut, Egypt [15]. The evaluation of the airflow characteristics comprises mean velocity and turbulence intensity distributions across the working section of the wind tunnel. In addition, the applicability of the wind tunnel to simulate the flow in the urban area atmospheres is verified by comparing the measured mean velocity against its counterpart obtained from Computational Fluid Dynamics (CFD) around and above buildings model.

2. EXPERIMENTAL SET-UP

2.1 The Atmospheric Boundary Layer Wind Tunnel

The wind tunnel used in the present work is a low-speed and open-loop type atmospheric boundary-layer wind tunnel that consists of the following eight components (see Fig. 1 for details) listed in order from front to back: (1) an upstream settling section, (2) a contraction cone (4:1 contraction ratio), (3) an air-flow heating unit, (4) an after heaters settling section, (5) a boundary layer development section, (6) a test section, (7) a transition and flexible connection, and (8) an axial flow fan. The effective working section is 1 m high, 1 m wide and 1.7 m long following a 3.5 m long development section just downstream of the boundary layer stimulation system. The flow uniformity is achieved by means of honeycomb and three screens. The honeycomb with 23 mm internal diameter and 230 mm long PVC tubes is used to reduce large turbulent eddies and lateral mean velocity variations. The eddies of the size of the honeycomb cell are then further broken down by the screens which are made of 54%, 45%, and 54%, open area ratios with mesh per inch counts of 12, 20, and 24, respectively. Three Irwin type vortex generators (spires) are placed at the

entrance of the boundary layer development section at equal spaces in the lateral direction [12]. An array of roughness elements were designed in a way to be a good simulation of real urban and industrial sites, which can be simply modeled as plan area occupied by uniformly distributed regular obstacles having the shape of cube. The boundary layer generated is about 0.5 m thick. The vertical velocity distribution in the test section, where the boundary layer is fully developed may be described by a power law as follows:

$$\frac{u}{u_\delta} = \left(\frac{z}{\delta}\right)^\alpha \tag{1}$$

where z, is the distance normal to the surface, u is the corresponding mean velocity, u_δ is the mean velocity at $z = \delta$ and δ is the boundary layer thickness. The vertical wind profile exponent α was estimated to be 0.28 [15]. The wind tunnel is driven by a 2 kW, 2 m^3/s axial flow fan. A maximum flow velocity of 2 m/s can be reached over the turntable.

2.2 The Measurements Technique

The measurements were carried out under neutral atmospheric conditions in the wind tunnel. Airflow characteristics in the wind tunnel have been assessed by measuring the vertical mean velocity and turbulence intensity distributions at the lateral centerline plane of the working section of the wind tunnel at different fan speeds and streamwise positions as shown in Fig. 2. The measurements were made using a spherical probe of Multi-Channel Anemometer (Model 1560, System 6243, Kanomax, Japan) connected to PC where the data are collected and analyzed using data acquisition software as shown in Fig. 1.

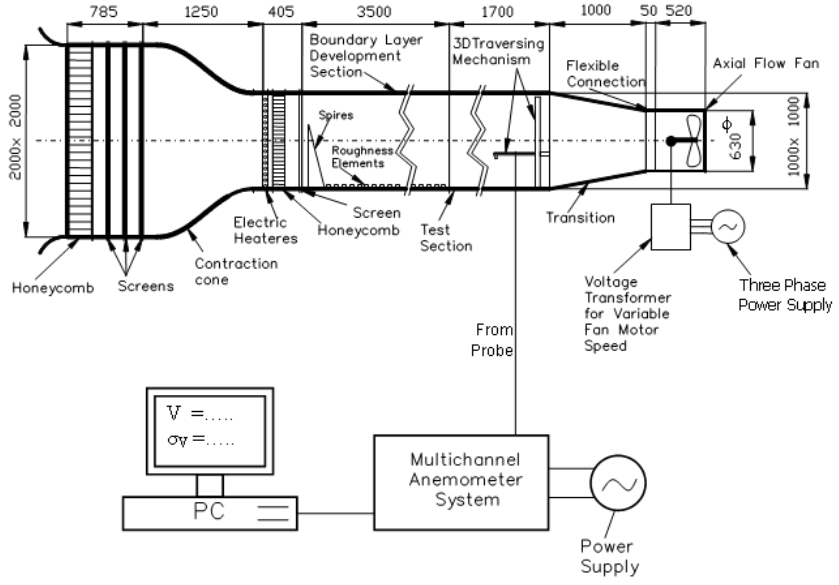

Figure 1: Main features and instrumentations of the atmospheric boundary layer wind tunnel (ABLWT) facility of Assiut University (dimensions in mm).

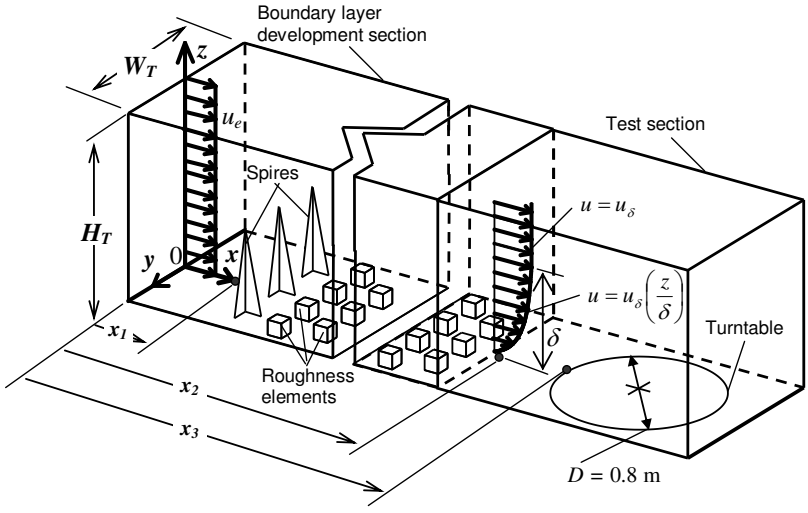

Figure 2: Conceptual model for the boundary layer development section and test section illustrating the coordinates system, velocity distributions, spires arrangement, arrays of roughness elements, and measuring positions.

2.3 The Physical Model

Building models are made of two wooden blokes. They are of uniform size 150 (H) × 150 (W) × 300 (L) mm. To select the model length scale, for low-rise building (below 100 m height), a good simulation can be achieved by omitting the gradient wind height and matching only the Jensen number as follows [16]:

$$\left(\frac{L_b}{z_0}\right)_{\text{model}} = \left(\frac{L_b}{z_0}\right)_{\text{prototype}} \tag{2}$$

where L_b is the characteristic dimension of the building and z_0 is the aerodynamic roughness length of the terrain which has a value in range of 0.4 − 0.7 m for dense low building [16]. Macdonald *et al.* [17] presented a formula to predict z_0 in the wind tunnels for uniform cube arrays which works over the full range of packing density. The calculated aerodynamic roughness length from Macdonald formula is 0.0028 m. According to the mentioned considerations, the calculated present model length scale is s = 1/200. The blocks are laid on the turntable floor perpendicularly and parallel to the flow direction to study two cases of model orientation namely for $\theta = 0^o$ and 90^o, where θ is the angle between the flow direction and the midplane between the two blocks of the model. Figure 3 illustrates the model configuration and measurement points locations.

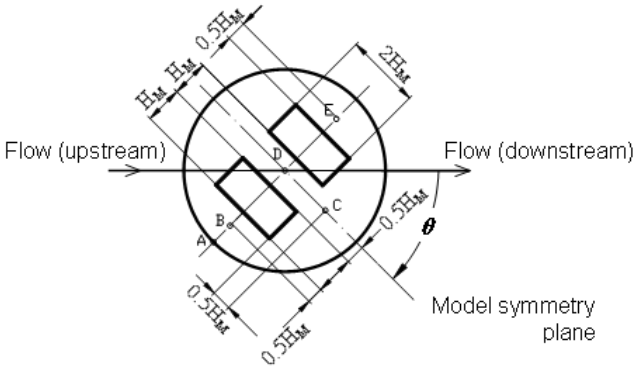

Figure 3: Orientation of the model with respect to the flow and measuring points.

3. MATHEMATICAL MODEL

3.1 Governing Equations

The fluid flow is modeled by partial differential equations describing the conservation of mass and momentum in 3D-dimensional Cartesian coordinates system for steady and incompressible flow. Numerical simulations are carried out through the CFD code, FLUENT® 6.3.26, based on a finite-volume discretization method and the geometry is modeled using GAMBIT® 2.3.16 software. The governing equations for the flow based on the Reynolds-averaged Navier–Stokes (RANS) approach with standard k-ε models are [18]:

Continuity equation:

$$\frac{\partial u_j}{\partial x_j} = 0 \tag{3}$$

Momentum equation:

$$\frac{\partial}{\partial x_j}(u_i u_j) = -\frac{1}{\rho}\frac{\partial p}{\partial x_i} + \frac{\partial}{\partial x_j}\left\{\nu\left(\frac{\partial u_i}{\partial x_j} + \frac{\partial u_j}{\partial x_i}\right) - \overline{u_i' u_j'}\right\} \tag{4}$$

where x_i are the Cartesian coordinates, ρ is the air density and v is its kinematic viscosity. u_i and p are the ith mean velocity component and mean static pressure, respectively. u_i' and u_j' are the fluctuating components of velocity, $\overline{u_i' u_j'}$ are the Reynolds stresses. The Reynolds stresses are parameterized as

$$-\overline{u_i' u_j'} = \nu_t\left(\frac{\partial u_i}{\partial x_j} + \frac{\partial u_j}{\partial x_i}\right) - \frac{2}{3}k\delta_{ij}, \tag{5}$$

$$\nu_t = c_\mu \frac{k^2}{\varepsilon} \tag{6}$$

where v_t is the turbulent kinematic viscosity of momentum, δ_{ij} is the kronecker delta (δ_{ij} = 1, if $i = j$, otherwise 0), k is the turbulent kinetic energy, ε is the dissipation rate of

the kinetic energy, and the c_μ is a constant having a value of 0.09 [19]. The turbulence kinetic energy, k, and its rate of dissipation, ε, are obtained from the following transport equations [19]:

$$\frac{\partial}{\partial x_j}(k\,u_j) = \frac{\partial}{\partial x_j}\left(\frac{\nu_t}{\sigma_k}\frac{\partial k}{\partial x_j}\right) + \nu_t\left(\frac{\partial u_i}{\partial x_j} + \frac{\partial u_j}{\partial x_i}\right)\frac{\partial u_i}{\partial x_j} - \varepsilon \tag{7}$$

$$\frac{\partial}{\partial x_j}(\varepsilon\,u_j) = \frac{\partial}{\partial x_j}\left(\frac{\nu_t}{\sigma_\varepsilon}\frac{\partial \varepsilon}{\partial x_j}\right) + c_{1\varepsilon}\frac{\varepsilon}{k}\nu_t\left(\frac{\partial u_i}{\partial x_j} + \frac{\partial u_j}{\partial x_i}\right)\frac{\partial u_i}{\partial x_j} - c_{2\varepsilon}\frac{\varepsilon^2}{k} \tag{8}$$

where $\sigma_k = 1.0$ and $\sigma_\varepsilon = 1.3$ are turbulent Prandtl numbers for k and ε, respectively, and $c_{1\varepsilon} = 1.44$ and $c_{2\varepsilon} = 1.92$ are constants [18, 19].

In modeling of urban flow, smaller grid size is desirable around building model to better resolve flow and dispersion field there. The above governing equations are solved numerically using a finite-volume method with the semi-implicit method for pressure-linked equation (SIMPLE) algorithm [20, 21]**.**

3.2 Model Specifications and Computational Domain

The model consists of two buildings each one has the dimensions of 30 m (H_M) × 30 m (W_M) × 60 m (L_M). The dimensions of the computational domain are large enough (690 m long (L_C), 360 m wide (W_C), and 180 m height (H_C)) to remove any significant influences of boundary conditions on the model [22]. Figure 4 shows the computational wind flow domain around and above the buildings together with the applied boundary conditions.

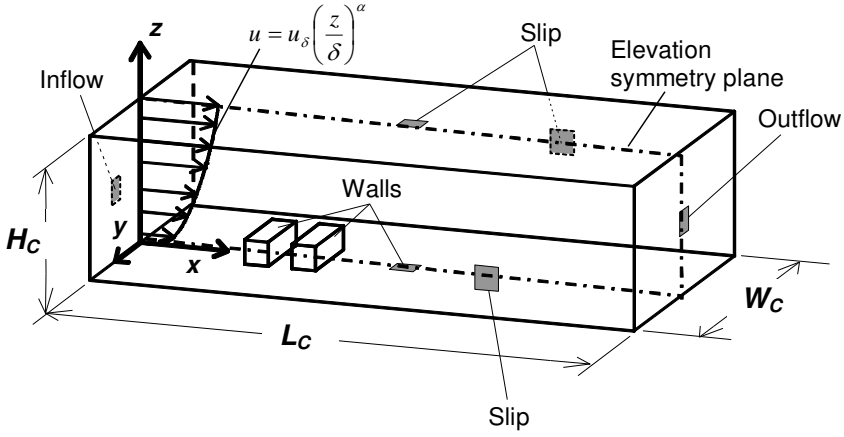

Figure 4: Computational domain, coordinate system, and boundaries.

3.3 Boundary conditions

***Inflow boundary*:** The inlet velocity profile for the atmospheric boundary layer is applied based on the power law (Eq. (1)) given above as:

$$\frac{u}{u_\delta} = \left(\frac{z}{\delta}\right)^{0.28} \tag{9}$$

At inlet, the turbulence kinetic energy, k, was formulated as in Eq. (10) [23] and the turbulent dissipation rate was calculated according to Eq. (11) which was given by the assumption of local equilibrium, i.e. the turbulent energy generated by the large eddies is distributed equally throughout the energy spectrum [23-25]:

$$k = \left[I(z) \times u(z)\right]^2 \tag{10}$$

$$\varepsilon = C_{\mu}^{1/2}\, k\,(z) \frac{u_{\chi}}{\delta} \alpha \left(\frac{z}{\delta}\right)^{\alpha-1} \tag{11}$$

where I is the turbulence intensity of the flow at the entrance of the test section (at x_2 = 3.53 m) and C_{μ} is a constant equal 0.09 .

***Sides and top boundaries*:** **S**lip boundary condition is used by **FLUENT** [26] when the physical geometry of interest and the expected pattern of the flow/thermal solution, has zero-shear slip walls in viscous flows. The slip condition is applied on the top and side boundaries as follows [27]:

at (x, W_C/2, z) and (x, - W_C/2, z) planes: $\mathrm{v} = 0$, $\dfrac{\partial(u, w, k, \varepsilon)}{\partial y} = 0$ (12)

at (x, y, H_C) plane: $w = 0$, $\dfrac{\partial(u, v, k, \varepsilon)}{\partial z} = 0$ (13)

***Outflow boundary*:** The boundary conditions used by **FLUENT** at outflow boundaries are; a zero diffusion flux for all flow variables and an overall mass balance correction. The zero diffusion flux condition applied by **FLUENT** at outflow boundaries is approached physically in fully-developed flows. Fully developed flows are flows in which the flow velocity profile (and/or profiles of other properties such as temperature) is unchanging in the flow direction [26]. The outflow boundary condition is applied on the domain outlet as follows [27]

at (L_C, y, z) plane: $p = p_0$, $\dfrac{\partial(u\ , k, \varepsilon)}{\partial x} = 0$ (14)

where p_0 is the atmospheric pressure.

***Wall boundaries*:** Wall function is employed in the near-wall region and a rough wall modification has been introduced as described in [27]. A roughness height has been taken as K_S =0.005 m.

4. RESULTS AND DISCUSSION

Air flow characteristics in the wind tunnel have been assessed by measuring the velocity and turbulence intensity distributions in the lateral vertical midplane at different streamwise positions. The measurements were performed for neutral wind flow under different fan speeds. The spherical probe used to measure the instantaneous velocity is attached to a computer controlled traversing mechanism for all measurements inside the test section. The measurements at the entrance of the boundary layer development section were carried out by the spherical probe attached to a simple manual traversing mechanism. The following discussions deal with the experimental results obtained for three groups of experiments. These are; experiments

in the empty wind tunnel, experiments in the wind tunnel with spires only, and experiments in the wind tunnel with the combination of spires and arrays of roughness elements. Figure 2 illustrates a plan view of the wind tunnel working section with measurements of wind tunnel characteristics axial positions. The measurements with the combination of spires and arrays of roughness elements were carried out in the empty test section and with existence of the buildings model. The measurements around and above the models were performed at two model orientations, namely at $\theta =$ 0^o and 90^o, as shown in Fig. 3. The results of measurements with existence of the model, are compared with CFD results as presented below.

4.1 Experiments in the Empty Wind Tunnel

Figure 5 shows the vertical distributions of the measured mean velocity and turbulence intensity obtained for empty wind tunnel at the entrance of the boundary layer development section (at x_1 of Fig. 2) for different fan speeds. The velocity distributions obtained at the entrance of the boundary layer development section show good uniformity across the whole height for all fan speeds, except for the boundary layer effect within about 4 cm above the lower smooth surface as shown in Fig. 5(a). Figure 5(b) shows that the turbulence intensity distributions are uniform across the whole height for all fan speeds and its normalized values are around 0.01.

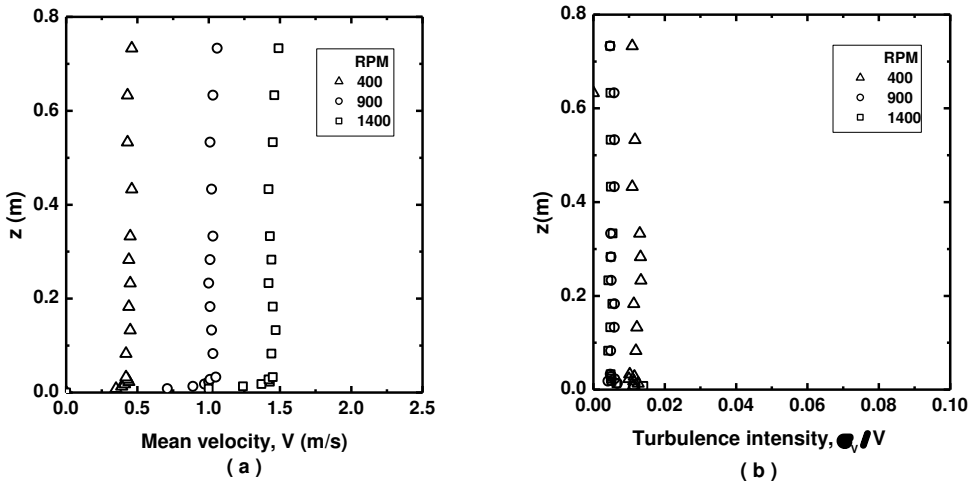

Figure 5: Vertical distributions of (a) mean velocity and (b) turbulence intensity, for empty wind tunnel at entrance of the boundary layer development section (x_1 = 0.1 m).

Figure 6(a) shows the vertical distributions of the measured mean velocity and power law fit obtained for empty wind tunnel at the entrance of the test section (at x_2 of Fig. 2) for different fan speeds. The values of the power law index, α, and boundary layer thickness, δ, vary the fan speed, thus it depends on the flow Reynolds number as shown in the figure. The boundary layer thickness, δ, decreases as the fan speed is increased, while the power law index, α, increases as the fan speed is increased. The obtained characteristics of the velocity distribution are that corresponding to the flow

over smooth flat plate. Figure 6(b) shows the vertical distributions of the turbulence intensity obtained at the same location and flow conditions. It is clear from this figure that the turbulence intensity normalized values converge to a value of about 0.01across the whole height for all fan speeds except near the wall where the wall effect is significant. Near the wall, the intensity is higher for lower fan speed and its value for different speeds decreases and gets closer to each other until it attains a constant value independent of the fan speed. Figures 5 and 6 confirm that the flow characteristics can be described by a uniform flow at the entrance of the boundary layer development section, and at the entrance of the test section, the boundary layer flow velocity profile can be described by power law whose parameter δ and α depend on Reynolds number. These flow characteristics are in agreement with results obtained and described in [28, 29].

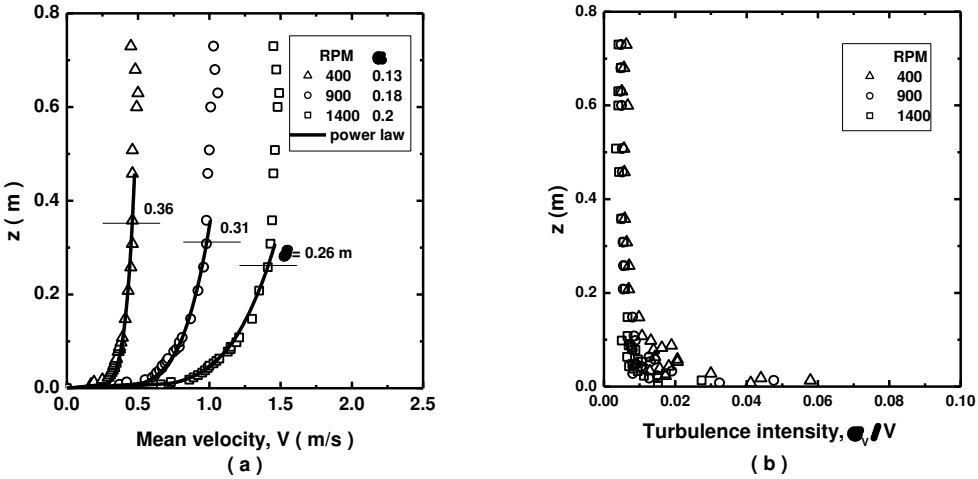

Figure 6: Vertical distributions of (a) mean velocity and (b) turbulence intensity, for empty wind tunnel at the entrance of the test section (x_2 = 3.53 m).

4.2 Experiments with Spires Only

Next, triangular spires with splitter plates (Fig. 2) are inserted into the wind tunnel. Figure 7 shows the vertical distributions of the measured mean velocity and turbulence intensity obtained for wind tunnel with spires at the entrance of the test section (at x_2 = 3.53 m, Fig. 2) for different fan speeds. The reason for adding the spires is to generate a thick boundary layer in a short distance. This can be clearly shown by comparing the measured mean velocity profiles without and with spires (Figs. 6 and 7, respectively) at the entrance of the test section. After installing spires, it is seen that the velocity profiles for the three fan speeds became similar to each other, and the boundary layer thickness grew from about 31 cm to 46 cm. The similarity of the three velocity profiles means that the flow regime is independent of the Reynolds number, which is an indication that the flow with spires is a fully developed turbulent flow. Using the power law to fit the measured data of Fig. 7(a) and considering a boundary layer thickness δ = 46 cm, an exponent of the power law α = 0.12 was obtained for all fan speeds considered in this study. These values of δ and α are for the measured velocity profiles shown in Fig. 7(a) which resulted from the effects of spires only. Figure 7(b)

shows that the turbulence intensity distributions are uniform outside the boundary layer for all fan speeds and its normalized values are around 0.01. Near the wall, the normalized values of turbulence intensity decrease with Reynolds number (fan speed) where the maximum normalized value near the bottom wall is about 0.10 for a fan speed of 400 rpm.

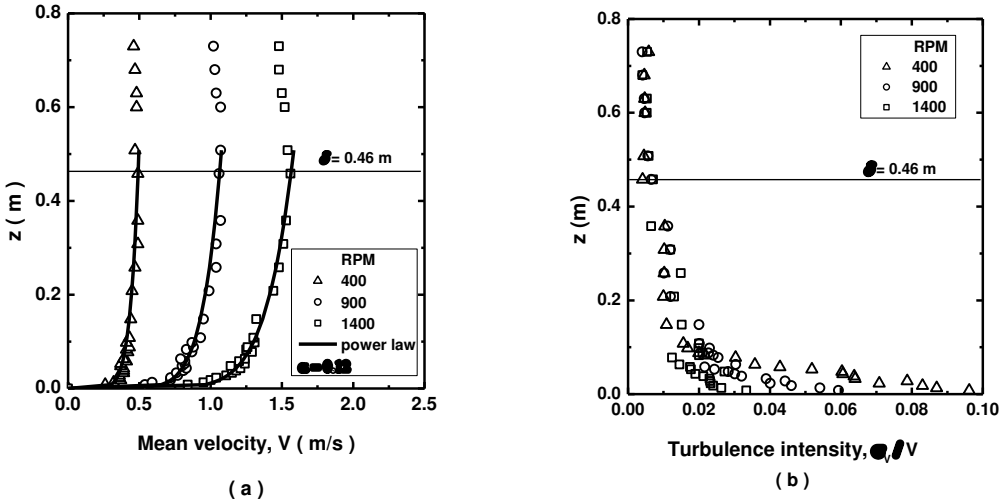

Figure 7: Vertical distributions of (a) mean velocity and (b) turbulence intensity, for the wind tunnel with spires only at entrance of the test section (x_2 = 3.53 m).

4.3 Experiments with Spires and Roughness Elements

Figure 8 shows the measured vertical distributions of the mean velocity and turbulence intensity for different fan speeds at the entrance of the test section with the combination of designed spires and arrays of roughness elements installed in the wind tunnel. As it is expected, the profiles indicate a simulated boundary layer thickness of about 51 cm. The boundary layer thickness is much thicker than before (shown in Fig. 7(a)) and slightly different from the design value of δ = 60 cm due to the manufacturing processes. The thick boundary layer is a direct result of the insertion of both spires and roughness elements. When the power law is used to fit the measured data of Fig. 8(a) with δ = 51 cm, an estimated value of the exponent α of 0.28 was obtained. The estimated value which corresponds to urban area condition is equal to the value of α = 0.28 used in the design of spires and roughness elements [15].

Although the experimental data of mean velocity distributions (see Figs. 6-8) show little scattering compared to the power law fit due to the combined effect of measuring and allocation errors, all the measured mean velocity profiles show the features of the main flow and boundary layer characteristics. The repetition of the main features for the mean velocity profiles, for different conditions, indicates the good reproducibility of the present wind tunnel.

Figure 8(b) shows that the turbulence intensity distributions are uniform outside the boundary layer for all fan speeds and its normalized values are around 0.01. Near the wall, the normalized values of turbulence intensity are higher compared to that of Fig. 7(b) where the maximum value near the bottom wall is about 0.15 for a fan speed of 400 rpm.

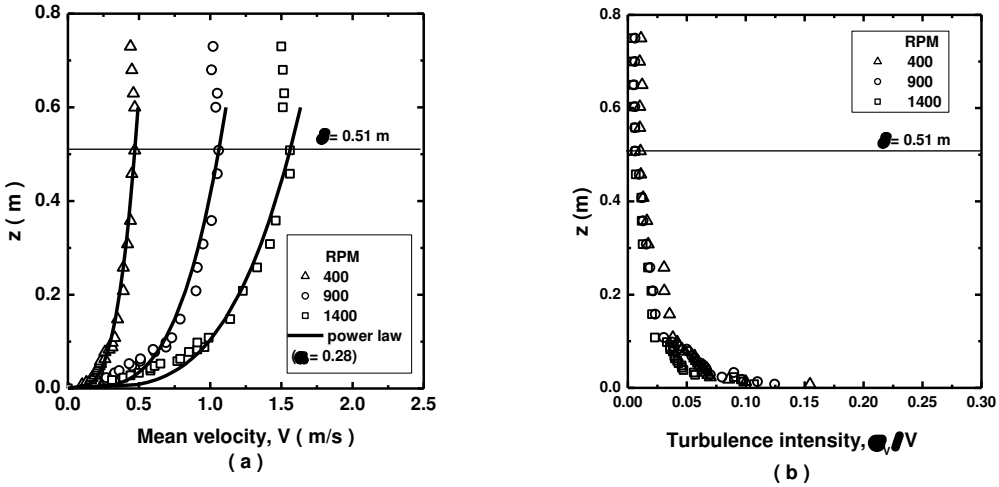

Figure 8: Vertical distributions of (a) mean velocity and (b) turbulence intensity, for the wind tunnel with spires and roughness elements (x_3 = 3.8 m).

Lateral distributions of mean velocity for different fan speeds at the entrance of the test section with the combination of designed spires and arrays of roughness elements installed in the wind tunnel were examined at vertical positions of 0.1, 0.2 and 0.3 m to check the uniformity of the flow in the wind tunnel central part. Uniformity of the mean velocity is observed within an accuracy of 5% over a central part of width about 75% of the wind tunnel width for all vertical positions and fan speeds as shown in Fig. 9. Therefore, the following measurements were made in the lateral midplane of the wind tunnel.

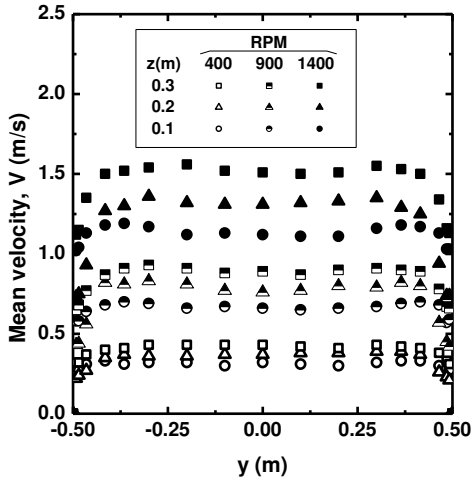

Figure 9: Lateral distributions of mean velocity with spires and roughness elements (x_3 = 3.8 m).

4.4 Comparison between Measured Mean Velocities and Turbulence Intensities around the Building Models with CFD Results.

Turbulent flow around and over a rough surface is an important problem in fluids engineering and has been the subject of numerous studies in diverse fields, such as aerodynamics, hydrodynamics, hydraulics, fluids machinery, atmospheric flows, and environmental studies [30]. Therefore an important part of the present study is to investigate the characteristics of the turbulent flow around buildings models located in roughened places. Figures 10-15 show the vertical distributions of the mean velocity and turbulence intensity for different fan speeds around the building models (θ = 90º) with the combination of designed spires and arrays of roughness elements installed in the wind tunnel. Moreover, a computational fluid dynamics (CFD) results for a full-scale model are presented and compared with the experimental one. Moreover, the computational fluid dynamics (CFD) results for a full scale model have been obtained and compared with the experimental one. Figure 10 shows the measured vertical distributions of the mean velocity along with the CFD results for different fan speeds obtained at point (A) upstream of the model (for θ = 90º). The experimental vertical distribution of the mean velocity obtained for fan speed of 400 rpm is similar to the numerical counterpart without velocity scaling shown as broken line in the figure. Although the velocity distributions are aerodynamically similar, they are different in values. These differences between the measured and computed values can be regarded to the followings: 1) the finite cross section dimensions of the wind tunnel compared to the real ABLs, 2) the effects of the wind tunnel walls, 3) the interference combined effects of the wind tunnel walls on the model walls, 4) the interruption effects of the measuring instrumentation in the wind tunnel, and 5) the arrangement of the system used for developing the boundary layer in the wind tunnel (spires and roughness elements which produce velocity distributions having a power law function deviation due to design constrictions, manufacturing arrangements especially near the wind tunnel floor simulating the Earth's surface). The deviation between the CFD and measurements can be minimized using a function form other than the power law. A simple linear function has been found to minimize that deviation. This explained by a velocity scale of (1/3) which has been selected to account for the differences between the measured velocities around the model and the corresponding full-scale velocities computed by CFD simulations. Figure 10 shows that the measured vertical distributions of the mean velocity agree well with the scaled velocities computed by CFD simulation for both fan speeds considered.

Figure 11(a) shows the measured vertical distributions of the mean velocity and turbulence intensity along with the CFD results for different fan speeds obtained at point (B) located at 0.5 H_H upstream of the model. The model existence disturbs the mean velocity and turbulence intensity distribution to a greater extent as shown. The mean velocity distributions at location (B) (Fig. 11a) upstream the model differ significantly compared with its counterpart before inserting the model (Fig. 7a). Figure 11(a) indicates that the flow decelerates as it approaches the model and that the streamwise mean velocity decreases near the bottom wall before it recovers again towards the edge of the boundary layer. The scaled velocity distributions computed by CFD indicate that the location of maximum velocity shifts toward the upper wall. This

distortion in the velocity distribution is believed to be a result of flow separation close to the model. The occurred separation zone contains eddies and reverse currents that definitely reduce the magnitude of the velocity in that region. Figure 11(a) shows that the measured vertical distributions of the mean velocity agree well both quantitatively and qualitatively with the scaled velocities computed by CFD simulation for both fan speeds considered.

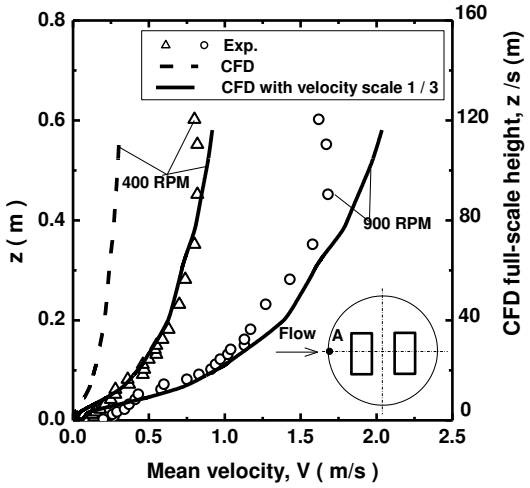

Figure 10: Vertical distributions of mean velocity at a location A upstream the model (θ = 90º).

Figure 11(b) shows that the turbulence intensity distributions tend to be uniform outside the boundary layer for all fan speeds, while it shows maximum values near the bottom wall corresponding to the vertical locations of the minimum mean velocities. The maximum normalized measured values are around 0.15 and 0.30 for the fan speed of 400 and 900 rpm, respectively. Moreover, Fig. 11(b) shows that the measured vertical distributions of the turbulence intensity agree well with the scaled intensities computed by CFD simulation for both fan speeds considered. Figure 11 shows that the numerical simulation is capable of predicting the deceleration (near the bottom wall) and acceleration of flow (towards the upper wall).

Figure 12 shows the measured vertical distributions of the mean velocity and turbulence intensity along with the CFD results for different fan speeds obtained at point (C) located on the side of the model midplane as shown in Fig. 3. The model existence disturbs the mean velocity and turbulence intensity distributions to a greater extent as shown. The mean velocity distributions at location (C) differ significantly compared with its counterpart upstream the model (at point (B)). Figure 11(a) shows also that the measured vertical distributions of the mean velocity agree well with the scaled velocities computed by CFD simulation for both fan speeds considered.

Figure 12(b) shows that the turbulence intensity distributions tend to be uniform outside the boundary layer for all fan speeds, while it shows maximum values near the bottom wall corresponding to the locations of the slow mean velocities (shown in Fig. 12(a)). The maximum measured values are around 0.17 and 0.23 for the fan

speed of 400 and 900 rpm, respectively. Figure 12 shows that the numerical simulation is capable of predicting the flow behavior at the side locations near the model.

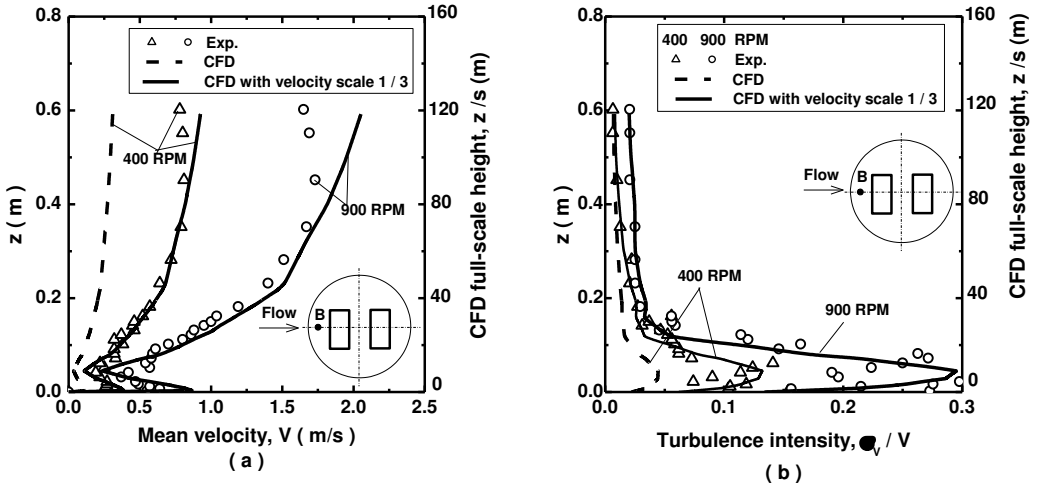

Figure 11: Vertical distributions of (a) mean velocity and (b) turbulence intensity, at a location B upstream the model (θ = 90º).

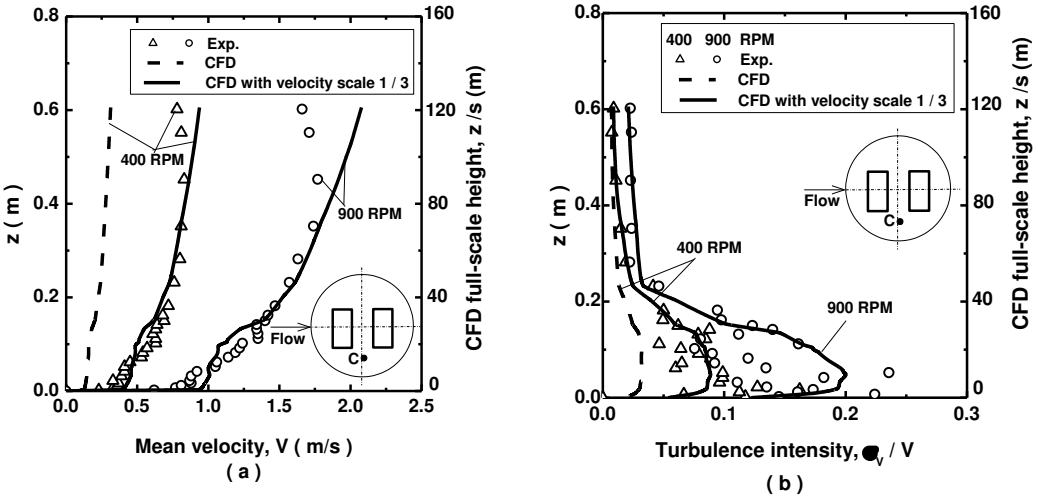

Figure 12: Vertical distributions of (a) mean velocity and (b) turbulence intensity, at a side location C (θ = 90º).

Figure 13 shows the measured vertical distributions of the mean velocity and turbulence intensity along with the CFD results for different fan speeds obtained at point (D) which is located at the center of the gap between the two buildings. The velocity distributions at the center of the model between the two buildings (gap profile) are well replicated both experimentally and numerically. Significant decrease in the magnitude of the mean velocity was experimentally detected and numerically predicted in the gap region as shown in the figure. This decrease starts to occur slightly above the model and becomes more significant in the gap between the two buildings. As

mentioned above, this drop in the mean velocity is a direct result of reverse currents and eddies expected to occur in the gap due to flow separation that takes place closely upstream the buildings in the gap between them and immediately downstream. Figure 13(a) shows that the measured vertical distributions of the mean velocity agree well with the scaled velocities computed by CFD simulation for both fan speeds considered.

Figure 13(b) shows that the turbulence intensity distributions tend to be uniform outside the boundary layer for all fan speeds, while it shows maximum values slightly far from the bottom wall. The intensity distributions predicted by CFD is closely replicated the experimental results where the shape of the experimental profiles is displayed. The maximum normalized values are around 0.10 and 0.20 for fan speeds of 400 and 900 rpm, respectively.

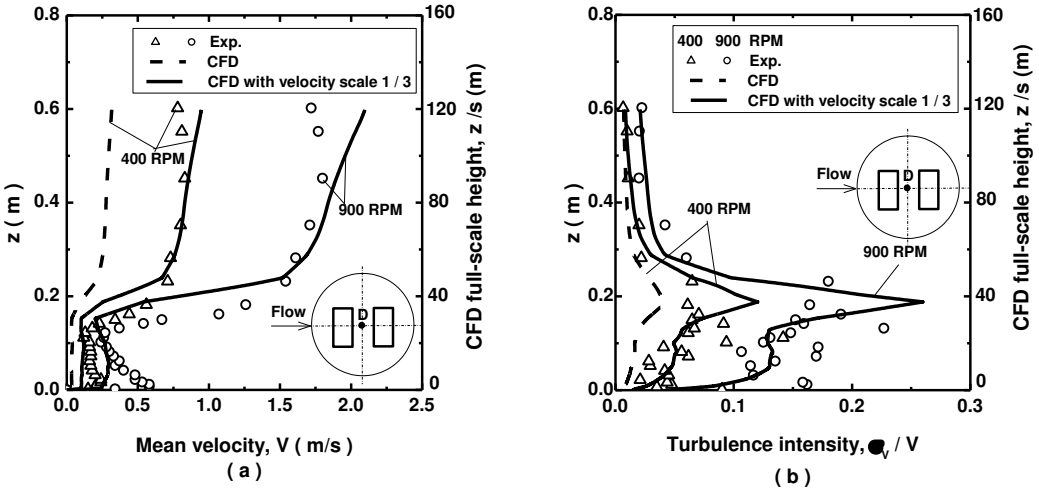

Figure 13: Vertical distributions of (a) mean velocity and (b) turbulence intensity, at the center location D of the model (θ = 90º).

Figure 14 shows the measured vertical distributions of the mean velocity along with the CFD results for different fan speeds obtained at point (E) downstream of the model. The velocity distributions downstream the buildings (wake profile) are well replicated both experimentally and numerically. Significant drop in the velocity flow was predicted in the wake region as shown in the figure. This drop in the mean velocities is a result of flow separation in the wake which is accompanied by reverse currents and eddies discussed above. Figure 14 shows that the measured vertical distributions of the mean velocity agree well with the scaled velocities computed by CFD simulation for both fan speeds considered.

Figure 15 shows contours of the mean velocity calculated by CFD with velocity scale 1/3 in the elevation symmetry plane. Measurements locations A, B, D and E at the upstream edge of the rotary table, upstream the model, between model buildings and downstream the model, respectively are also shown. The figure clearly shows the separation zones that occur upstream the buildings, in the gap between them and downstream. Contours far above the model height are nearly parallel. The figure shows that vortex fills the cavity between the two buildings (point D). This vortex prevents the outer flow from reattaching to the wind tunnel floor within the cavity

between the two buildings. Streamlines above the cavity are still nearly parallel except near the buildings. Flow reattaches to the wind tunnel floor far downstream the model. The reattachment point is located downstream the buildings at about four times the building height. Though contours far away from the model buildings are nearly parallel, in the lower half of the wind tunnel they undulate in response to model geometry. These results are qualitatively agree well with the numerical results obtained by Hamlyn and Britter [31].

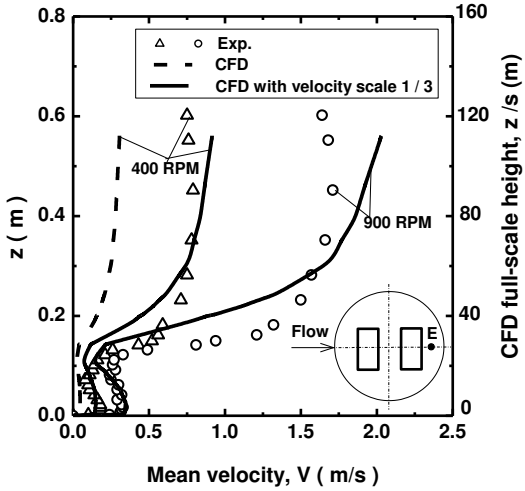

Figure 14: Vertical distributions of mean velocity at a location E downstream of the model (θ = 90 º).

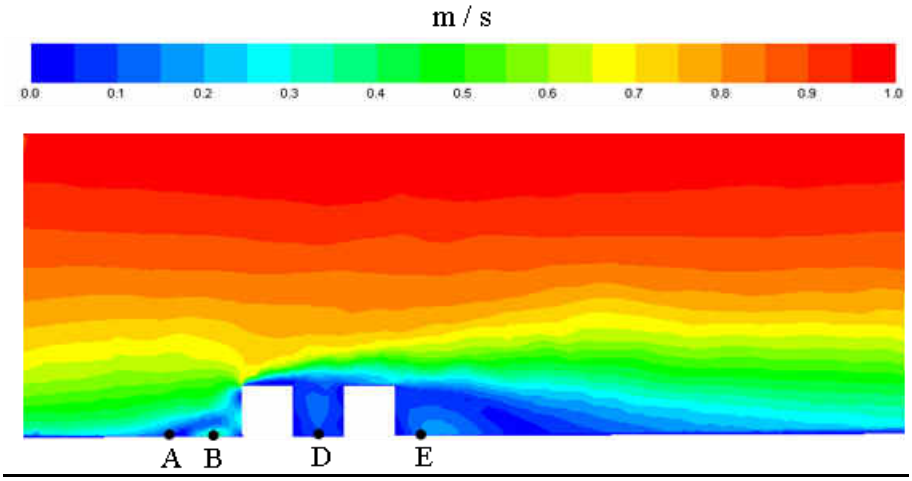

Figure 15: Contours of mean velocity calculated by CFD with velocity scale 1 / 3, in the elevation symmetry plane (θ = 90 º, u_δ at 400 RPM).

Previous wind tunnels measurements and Computational Fluid Dynamics (CFD) simulations have led to the common knowledge that wind speed values in passages between buildings significantly increased [32]. Different types of passages between buildings can be distinguished such as passages between parallel buildings

that are placed side-by-side. The importance of such studies in the field of atmospheric flows is obvious particularly regarding the pollutants distributions and dispersions. Figures 16-19 show the vertical distributions of the mean velocity and turbulence intensity for different fan speeds around the building models (parallel buildings, $\theta = 0°$) with the combination of designed spires and arrays of roughness elements installed in the wind tunnel. Moreover, a computational fluid dynamics (CFD) results for a full scale model are presented and compared with the corresponding experimental results. Model validation is performed for the situation with two buildings of equal height and for wind direction parallel to the centre line of the passage between them.

Figure 16 shows the measured vertical distributions of the mean velocity and turbulence intensity along with the CFD results for a fan speed of 400 rpm obtained at point (B) located at the side of the buildings model. The model existence disturbs the mean velocity and turbulence intensity to a greater extent particularly near the bottom wall as shown. Figure 16(a) shows that the mean velocity distribution at location (B) is similar to its counterpart shown in Fig. 12(a) where the mean velocity is accelerated near the bottom wall due to the venture effect. Figure 16(a) shows that the measured vertical distribution of the mean velocity agrees well with the scaled velocities computed by CFD simulation.

Figure 16(b) shows that the turbulence intensity distribution tends to be uniform outside the boundary layer, while it shows maximum values near the bottom wall. The maximum normalized values are around 0.10. Moreover, Fig. 16(b) shows that the measured vertical distribution of the turbulence intensity agrees well with the scaled intensities computed by CFD simulation.

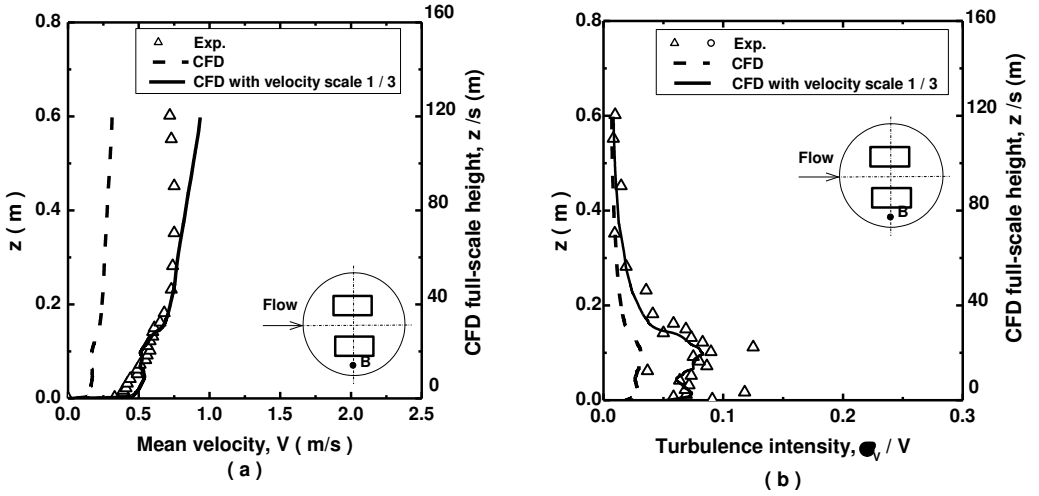

Figure 16: Vertical distributions of (a) mean velocity and (b) turbulence intensity, at a side location B of the model (θ = 0º at 400 RPM).

Figures 17 and 18 shows the measured vertical distributions of the mean velocity and turbulence intensity along with the CFD results obtained at points (C) and (D) downstream and between the model buildings, respectively. Both Figures show that the mean velocity distributions are similar where the mean velocity is accelerated near the bottom wall due to the venture effect. However, the velocity increase near the

wall is more pronounced at point (D) compared with that at (C). Figures 16(a) and 17(a) show that the measured vertical distributions of the mean velocity agree well with the scaled velocities computed by CFD simulation.

Figures 17(b) and 18(b) show that the turbulence intensity distributions are uniform outside the boundary layer, while they show maximum values near the bottom wall. The maximum normalized values are around 0.10 in both cases. Moreover, the figures show that the measured vertical distributions of the turbulence intensity agree well both quantitatively and qualitatively with the scaled normalized intensities computed by CFD simulation.

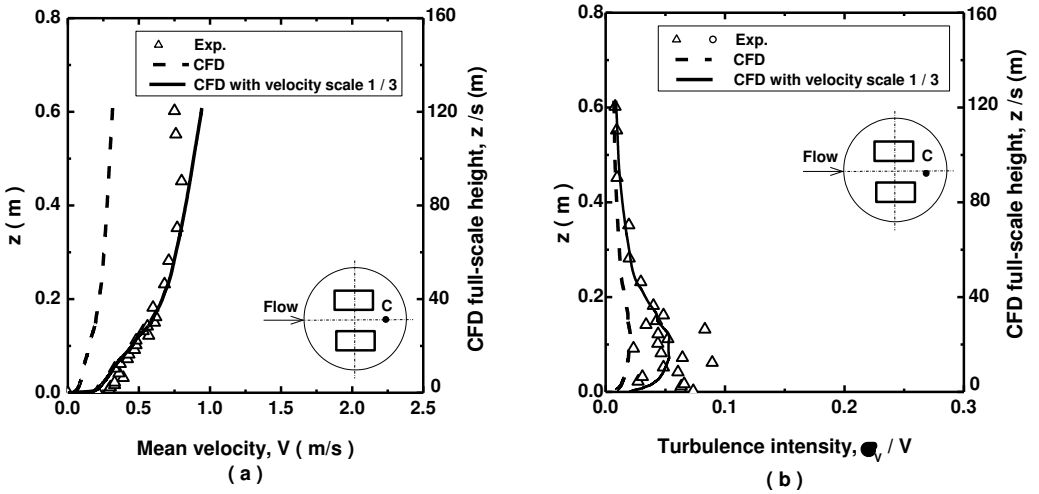

Figure 17: Vertical distributions of mean velocity at a location C downstream of the model (θ = 0º at 400 RPM).

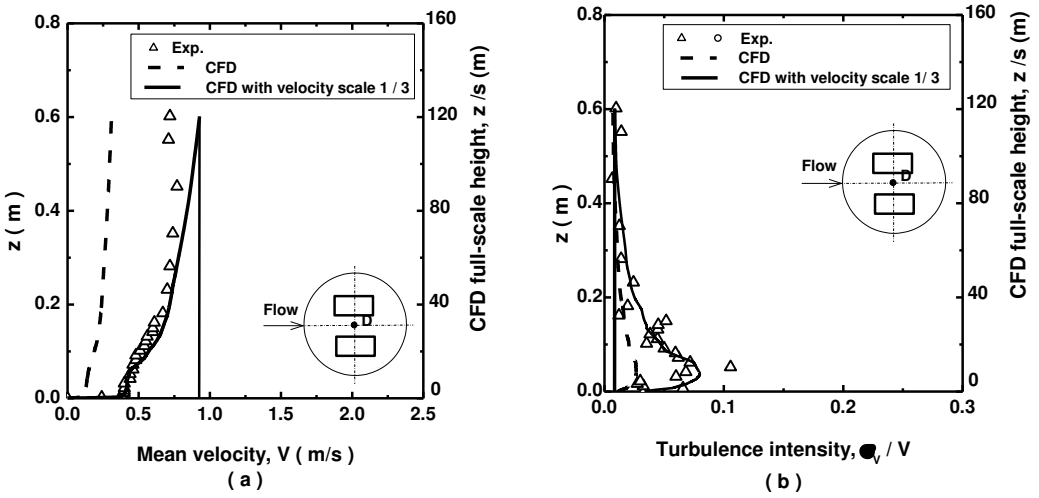

Figure 18: Vertical distributions of (a) mean velocity and (b) turbulence intensity, at the center location D of the model (θ = 0º at 400 RPM).

Figure 19 shows contours of the mean velocity calculated by CFD with velocity scale 1/3 in the lateral plane. Measurements locations B and D (point C is located along the line with point D) at the side of the model and between model buildings, respectively are also shown. The point (C) is not shown in Fig. 19 because it is located in a plane downstream that of in which points (B) and (D) are located. Contours far above the model height are nearly parallel. A relatively high velocity fills the passage between the two buildings (point D) and at the sides of the model buildings. This can be attributed to the venture effect as the flow area is decreased at this section. Though contours far away from the model buildings are nearly parallel, in the lower half of the wind tunnel they are small at the vicinity of the model building walls. These results are qualitatively in accordance with numerical results obtained by Blocken *et al*. [32].

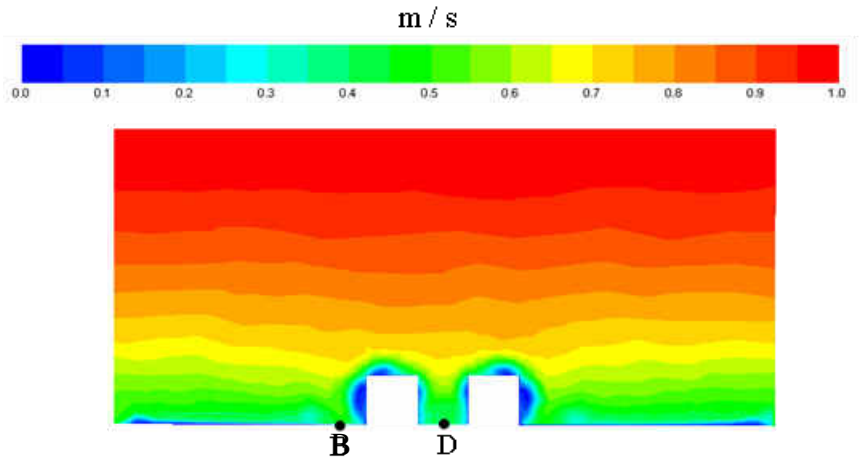

Figure 19: Contours of mean velocity calculated by CFD with velocity scale 1 / 3, in the lateral plane at x = 180 m, (θ = 0º, u_δ at 400 RPM).

5. CONCLUSIONS

A new low-speed boundary-layer wind tunnel has been designed and constructed at the University of Assiut. A series of flow-characteristic evaluations were performed in this wind tunnel to determine the uniformity of flow and to verify its adequacy to simulate the atmospheric boundary layer (ABL) for environmental flow studies and pollutants dispersion in urban atmospheres. Measurements of mean velocity and turbulence intensity in the wind tunnel were conducted using spherical probe of Multi-Channel Anemometer. The simulation of the ABL was carried out using the Irwin's method that consists of a combination of spires and roughness elements. In addition, the applicability of the wind tunnel to simulate the flow in the urban area atmospheres has been verified by comparing the measured mean velocity and turbulence intensity distributions against with the corresponding distributions obtained from Computational Fluid Dynamics (CFD) around and above buildings model. The following conclusions can be drawn:

1. The measurements showed uniform velocity distributions and low turbulence intensities at the entrance of boundary development section in the empty wind tunnel.
2. The simulated ABL at the entrance of the test section has a thickness of up to 500 m corresponding to urban area.
3. The experimental results showed that the present wind tunnel is capable to maintain long run steady flow characteristics and reproducible flow patterns.
4. For the building configuration normal to wind direction, the flow through elevation plane is characterized by gap (between model buildings) and wake (downstream model buildings) flows. Flow separation in these zones and reattachment downstream the wake have been accurately detected.
5. For the building configuration parallel to wind direction, the flow through a lateral vertical plane in the passages is slightly higher than the flow rate through a similar vertical plane in free-field conditions (with no buildings).
6. Numerical results obtained from CFD around and above buildings model agree well with the experimental data giving confidence in extending the CFD computations in future applications concerning the atmospheric flows.

REFERENCES

[1] Cook, N. J., "A Boundary Layer Wind Tunnel for Building Aerodynamics", J. of Wind Engineering and Industrial Aerodynamics, Vol. 1, No. 1, 1975, pp. 3-12.

[2] Sykes, D. M., "A New Wind Tunnel for Industrial Aerodynamics", J. of Wind Engineering and Industrial Aerodynamics, Vol. 2, No. 1, 1977, pp. 65-78.

[3] Counihan J., "An Improved Method of Simulating an Atmospheric Boundary Layer in a Wind Tunnel", J. of Atmospheric Environment, Vol. 3, No. 2, 1969, pp. 197-200.

[4] Blessmann, J., "The Boundary Layer TV-2 Wind Tunnel of the UFRGS", J. of Wind Engineering and Industrial Aerodynamics, Vol. 10, No. 2, 1982, pp. 231-248.

[5] Hansen, S. O. and Sorensen, E. G., "A New Boundary Layer Wind Tunnel at the Danish Maritime Institute", J. of Wind Engineering and Industrial Aerodynamics Vol. 18, No. 2, 1985, pp. 213-224.

[6] Garg, R. K., Lou, J. X. and Kasperski, M., "Some Features of Modeling Spectral Characteristics of Flow in Boundary Layer Wind Tunnels", J. of Wind Engineering and Industrial Aerodynamics, Vol. 72, No. 1, 1997, pp. 1-12.

[7] Farell, C. and Iyengar, A. K. S., "Experiments on the Wind Tunnel Simulation of Atmospheric Boundary Layers", J. of Wind Engineering and Industrial Aerodynamics, Vol. 79, No. 1-2, 1999, pp. 11-35.

[8] Wittwer, A. R. and Moller, S. V., "Characteristics of the Low-Speed Wind Tunnel of the UNNE", J. of Wind Engineering and Industrial Aerodynamics, Vol. 84, No. 3, 2000, pp. 307-320.

[9] De Bortoli, M. E., Natalini, B., Paluch, M. J., and Natalini, M. B., "Part-Depth Wind Tunnel Simulations of the Atmospheric Boundary Layer", J. of Wind Engineering and Industrial Aerodynamics, Vol. 90, No. 4-5, 2002, pp. 281-291.

[10] Balendra, T., Shah, D. A., Tey, K. L. and Kong, S. K., "Evaluation of Flow Characteristics in the NUS-HDB Wind Tunnel", J. of Wind Engineering and Industrial Aerodynamics, Vol. 90, No. 6, 2002, pp. 675-688.

[11] Counihan, J., "Simulation of an Adiabatic Urban Boundary Layer in a Wind Tunnel", J. of Atmospheric Environment, Vol. 7, No. 7, 1973, pp. 673-689.

[12] Irwin, H. P. A. H., "The Design of Spires for Wind Simulation", J. of Wind Engineering and Industrial Aerodynamics, Vol. 7, No. 3, 1981, pp. 361-366.

[13] Cook, N. J., "On Simulating the Lower Third of the Urban Adiabatic Boundary Layer in a Wind Tunnel", J. of Atmospheric Environment, Vol. 7, No. 7, 1973, pp. 691-705.

[14] Standen, M. M., "A Spire Array for Generating Thick Turbulent Shear Layers for Natural Wind Simulation in Wind Tunnels", National Research Council of Canada, NAE Report LTR-LA-94, 1972.

[15] Al-Nehari, H. A., Ali K. Abdel-Rahman, Nassib, A. E. and Shafey, H. M., "Design and Construction of a Wind Tunnel for Environmental Flow Studies", Cairo 11th International Conference on Energy and Environment, Hurghada, Egypt – March 15-18, 2009.

[16] American Society of Civil Engineers, "Wind Tunnel Studies of Building and Structures", ASCE Manuals and Reports on Engineering, Practice No. 67, 1999.

[17] Macdonald, R. W., Griffiths, R. F. and Hall, D. J., "An Improved Method for Estimation of Surface Roughness of Obstacle Arrays", J. of Atmospheric Environment, Vol. 32, No. 11, 1998, pp. 1857-1864.

[18] Launder, B. E., and Spalding, D. E., "The Numerical Computation of Turbulent Flows", J. of Computer Methods in Applied Mechanics and Engineering Vol. 3, No. 2, 1974, pp. 269-289.

[19] Maele, K. V., and Merci, B., "Application of Two Buoyancy-Modified k–ε Turbulence Models to Different Types of Buoyant Plumes", J. of Fire Safety, Vol. 41, No. 2, 2006, pp. 122-138.

[20] Baik, J., Kim, J. and Fernando, J. S., "A CFD Model for Simulating Flow and Dispersion", J. of Applied Meteorology, Vol. 42, 2003, pp. 1636-1648.

[21] Patanker S.V. "Numerical Heat Transfer and Fluid Flow", McGraw-hill Ed. 5, 1980.

[22] Mochida, A., Tominaga, Y., and Yoshie, R., "AIJ Guideline for Practical Applications of CFD to Wind Environment Around Buildings", The fourth International Symposium on Computational Wind Engineering (CWE2006), Yokohama, Japan, 2006.

[23] Kondo, H., Horiuchi, K., Hirano, Y., Maeyama, N., Ogat, K., Iizuka S., and Mizuno, T., "Attempt to Make Guideline to use CFD Model for Atmospheric Environmental Assessment in Urban Area in Japan", The Seventh International Conference on Urban Climate, 29 June - 3 July 2009, Yokohama, Japan.

[24] Norton, T., Grant, J., Fallon, R., and Sun, D., "Optimising the Ventilation Configuration of Naturally Ventilated Livestock Buildings for Improved Indoor Environmental Homogeneity", J. of Building and Environment, Vol. 45, No. 4, 2010, pp. 983-995.

[25] Kim, T., Kim, K., Kim, B. S., "A Wind Tunnel Experiment and CFD Analysis on Airflow Performance of Enclosed-Arcade markets in Korea", J. of Building and Environment, Vol. 45, No. 5, 2010, pp. 1329-1338.

[26] Fluent Inc., FLUENT 6.3.26 user Manual, (2006).
[27] Yang, W., Quan, Y., Jin, X., Tamura, Y., and Gu, M., "Influences of Equilibrium Atmosphere Boundary Layer and Turbulence Parameter on Wind Loads of Low-Rise Buildings", J. of Wind Engineering and Industrial Aerodynamics Vol. 96, No. 10-11, 2008, pp. 2080-2092.
[28] Ohya, Y., Tatsuno, M., Nakamura, Y., and Ueda, H., "A Thermally Stratified Wind Tunnel for Environmental Flow Studies", J. Atmospheric Environment, Vol. 30, No. 16, 1996, pp. 2881-2887.
[29] Wang, M., "Application of Laser Doppler Velocimetry to Measurement of the Velocity Field Close to Regularly Arrayed Rough surfaces", Ph. D. Thesis, Chemical Engineering, University of Arkansas, USA, 2006.
[30] Cui J., Virendra C. P. and Ching-Long L., "Large-Eddy Simulation of Turbulent Flow in a Channel With Rib Roughness", International Journal of Heat and Fluid Flow, Vol. 24, 2003, pp. 372–388.
[31] Hamlyn D. and Britter R. "A Numerical Study of the Flow Field and Exchange Processes within a Canopy of Urban-Type Roughness", J. of Atmospheric Environment, Vol. 39, 2005, pp. 3243-3254.
[32] Blocken, B., Carmeliet J. and Stathopoulos T., "CFD Evaluation of Wind Speed Conditions in Passages Between Parallel Buildings - Effect of Wall-Function Roughness Modifications for the Atmospheric Boundary Layer Flow", Journal of Wind Engineering and Industrial Aerodynamics, Vol. 95, 2007, pp. 941–962.

خصائص نفق الرياح منخفض السرعة المستخدم لمحاكاة الأجواء الحضرية

م. حمود النهاري ، د. على كامل عبد الرحمن ، أ.د. حمدي معوض شافعي و د. عبد المنعم نصيب

أجريت هذه الدراسة لغرض التشخيص والتقييم لخصائص الانسياب داخل نفق الرياح الذي تم تصميمه وإنشاؤه مسبقا في معامل جامعة أسيوط لدراسة التدفقات البيئية. لتحقيق ذلك أجريت سلسلة من القياسات لإثبات انتظام الانسياب ومقدرة نفق الرياح لمحاكاة طبقة الجو الحدودية من أجل دراسة التدفقات البيئية المختلفة وانتشار الملوثات في جو المناطق الحضرية. يعرض هذا البحث لنتائج القياسات المعملية لتوزيعات السرعة المتوسطة وشدة الاضطراب للانسياب عند قيم مختلفة لسرعات المروحة الدورانية. بينت القياسات انتظام السرعات المتوسطة وانخفاض شدة الاضطراب للانسياب عند مدخل القطاع المخصص لإنتاج ومحاكاة طبقة الجو الحدودية. يصل سمك هذه الطبقة في المناطق الحضرية إلى 500 متر. تم محاكاة هذه الطبقة داخل نفق الرياح باستخدام مجموعة مؤتلفة من عوارض مدببة مثلثة الشكل بالإضافة إلى مصفوفة من عناصر خشونة مكعبة الشكل. أظهرت نتائج القياسات المعملية التي أجريت لفترات طويلة أن نفق الرياح يمكنه استعادة النتائج التي تم الحصول عليها والحفاظ على استقرار خصائص السريان لنفس الظروف. مقدرة نفق الرياح في محاكاة الانسياب في المناطق الحضرية تم التحقق منها بمقارنة نتائج القياسات المعملية بالنتائج المناظرة لها باستعمال نماذج ديناميكيا الموائع الحسابية بدراسة الانسياب بالقرب من نموذج يمثل مبنيين في منطقة حضرية. أثبتت الدراسة أنه يوجد توافق بين نتائج استخدام نماذج المحاكاة العددية، وتلك التى تم الحصول عليها عملياً.